JOURNAL OF GEOPHYSICAL RESEARCH, VOL. 112, D07309, doi:10.1029/2006JD007904, 2007

Observational characteristics of double tropopauses

William J. Randel,[1] Dian J. Seidel,[2] and Laura L. Pan[1]

Received 10 August 2006; revised 29 November 2006; accepted 21 December 2006; published 11 April 2007.

[1] Temperature profiles in the extratropics often exhibit multiple tropopauses (as defined using the lapse rate definition). In this work we study the observational characteristics of double tropopauses based on radiosondes, ERA40 reanalysis, and GPS radio occultation temperature profiles. Double tropopauses are associated with a characteristic break in the thermal tropopause near the subtropical jet, wherein the low latitude (tropical) tropopause extends to higher latitudes, overlying the lower tropopause; this behavior can extend to polar latitudes. Tropopause statistics derived from radiosondes and GPS data show good agreement, and GPS data allow mapping of double tropopause characteristics over the globe. The occurrence frequency shows a strong seasonal variation over NH midlatitudes, with ~50–70% occurrence in profiles during winter, and a small fraction (~10%) over most of the hemisphere during summer (with the exception of a localized maximum over the poleward flank of the Asian monsoon anticyclone). SH midlatitude statistics show a smaller seasonal variation, with occurrence frequencies of ~30–50% over the year (maximum during winter). Over the extratropics, the occurrence frequency is substantially higher for cyclonic circulation systems. Few double tropopauses are observed in the tropics. Ozone measurements from balloons and satellites show that profiles with double tropopauses exhibit systematically less ozone in the lower stratosphere than those with a single tropopause. Together with the meteorological data, the ozone observations identify double tropopauses as regions of enhanced transport from the tropics to higher latitudes above the subtropical jet cores.

Citation: Randel, W. J., D. J. Seidel, and L. L. Pan (2007), Observational characteristics of double tropopauses, *J. Geophys. Res.*, *112*, D07309, doi:10.1029/2006JD007904.

1. Introduction

[2] Behavior of the global tropopause relates to questions in dynamic meteorology, stratosphere-troposphere exchange (STE), and climate variability and change. The tropopause is recognized as a key feature of atmospheric structure in both the midlatitudes [*Hoskins et al*, 1985] and the tropics [*Reid and Gage*, 1996], and an overall understanding of STE is dependent on an ability to quantify tropopause structure and variability [e.g. *Holton et al*., 1995; *Shepherd*, 2002; *Stohl et al*., 2003]. Low frequency variations of the tropopause are closely coupled to stratospheric ozone changes [*WMO*, 2003], and furthermore *Sausen and Santer* [2003] and *Santer et al.* [2003] have suggested that changes in the height of the tropopause may be a sensitive indicator of anthropogenic climate change. Thus enhanced understanding of tropopause behavior can contribute to a number of topics.

[3] In simple terms, the tropopause marks the boundary between the troposphere and stratosphere, and a fundamental characteristic of the tropopause is a change in static stability (temperature lapse rate) across the interface. The *WMO* [1957] definition of the tropopause is based on lapse rate criteria, although the tropopause can also be defined by more general stability criteria, quantified by potential vorticity (PV) [e.g. *Hoerling et al.*, 1991]. In the tropics the tropopause is relatively high (~16 km), reflecting a transition between radiative-convective balance in the troposphere and radiative balance in the stratosphere [*Thuburn and Craig*, 2002]. The tropopause in the extratropics is lower (~8–12 km), with an equilibrium structure determined by baroclinic wave dynamics [*Held*, 1982; *Haynes et al*., 2001; *Schneider*, 2004]. The extratropical tropopause is characterized by large dynamic variability, often with complex spatial structure [such as three-dimensional folds, e.g. *Bithel et al.*, 1999; *Nielsen-Gammon*, 2001].

[4] In terms of the lapse rate tropopause, the interface between the tropics and extratropics at a particular longitude is often characterized by a split in the tropopause (coincident with the subtropical jet stream), rather than a continuous transition [e.g. *Kochanski*, 1955]. Over this region, soundings can reveal the existence of multiple tropopauses. *Seidel and Randel* [2006] used historical radiosonde data to quantify variability and trends in the global tropopause, and found that a large fraction of midlatitude soundings during winter exhibited multiple tropopauses [also noted in Argentine radiosonde data by *Bischoff et al.* [2007], and in GPS data by *Schmidt et al.* [2006]. The presence of multiple stable layers and multiple tropopauses in the upper tropo-

[1]National Center for Atmospheric Research, Boulder, Colorado, USA.
[2]NOAA Air Resources Laboratory, Silver Spring, Maryland, USA.

0148-0227/07/2006JD007904$09.00

sphere/lower stratosphere (UTLS) region has been known since the advent of upper air soundings [e.g. *Bjerknes and Palmen*, 1937; *Kochanski*, 1955], and their synoptic structure was studied systematically during the 1970s using research aircraft observations [e.g. *Shapiro*, 1978; *Keyser and Shapiro*, 1986]. These studies highlighted the relationships between upper tropospheric frontal layers and tropopause folds, the latter identified by PV and ozone distributions [*Shapiro*, 1980; *Browell et al.*, 1987]. More recently, the double tropopause phenomenon has been discussed in relation to ozone variability in *Varotsos et al.* [2004] and *Pan et al.* [2004]. However, while the existence of double tropopauses has been documented, there have been few systematic studies of their observational characteristics or climatology, and their relevance for understanding dynamical and chemical transitions between the troposphere and stratosphere. In this work we seek an improved characterization of atmospheric structure associated with double tropopauses, which should serve as a first step toward understanding controlling mechanisms and their relevance to the topics discussed above.

[5] This paper has several components. First, the behavior and global climatology of double tropopauses is studied based on temperature profiles from radiosondes, GPS radio occultation measurements (hereafter GPS), and ERA40 reanalysis data. We use the high vertical resolution of radiosondes and GPS data, together with global sampling of GPS, to quantify the space-time variability of double tropopause occurrences. The ERA40 meteorological data (winds and temperatures) are used to analyze the large-scale dynamic structure associated with double tropopauses for a few examples. We also analyze the statistical relationships between tropopause behavior and upper tropospheric circulation, as quantified by relative vorticity at 200 hPa. Furthermore, ozone variability associated with double tropopauses is studied based on balloon and satellite observations. Together with the meteorological analyses, the ozone data are used to characterize transport behavior associated with double tropopauses. We also comment briefly on long-term variability of double tropopause statistics.

2. Data and Analyses

2.1. Radiosondes

[6] The radiosonde data used here are obtained from the Integrated Global Radiosonde Archive [*Durre et al.*, 2006] at the NOAA National Climatic Data Center (NCDC). We focus on a set of 50 stations over the globe discussed in detail in *Seidel and Randel* [2006], that were selected based on the length and completeness of their archived data record, homogeneity characteristics and global coverage. The individual sounding profiles are used to determine the location of the first lapse-rate tropopause (LRT, or LRT1) and, if present, the second (or third) tropopause (LRT2, LRT3), using the definition from the World Meteorological Organization's Commission for Aerology [*WMO*, 1957].

[7] The *first tropopause* is defined as the lowest level at which the lapse rate decreases to 2°C/km or less, provided also the average lapse rate between this level and all higher levels within 2 km does not exceed 2°C/km.

[8] If above the first tropopause the average lapse rate between any level and all higher levels within 1 km exceeds 3°C/km, then a *second tropopause* is defined by the same criterion as under (a). This tropopause may be either within or above the 1 km layer.

[9] The vertical resolution of radiosonde data has increased over time, with typically ~40 reported data levels between 700 and 50 hPa in recent decades, or ~0.5 km resolution. However, the reported levels are not evenly spaced but include data at fixed mandatory pressure levels and so-called significant levels, at which the data depart from linearity between the two nearest mandatory levels.

2.2. GPS Data

[10] The high vertical resolution and high accuracy of GPS radio occultation temperature measurements was demonstrated by the GPS/MET satellite, which collected data during April 1995–February 1997 [*Kursinski et al.*, 1996; *Rocken et al.*, 1997]. In this work we use GPS data from two follow-on satellite instruments, CHAMP [*Wickert et al.*, 2005; data available 2001–2005] and SAC-C (data available 2001–2002). *Hajj et al.* [2004] have extensively characterized and compared the CHAMP and SAC-C temperature retrievals, and demonstrated that individual profiles are precise to <0.6 K over 5–15 km, increasing to ~2 K at 25 km. The vertical resolution of GPS retrievals can approach ~100 m, but the data used here are sampled on a 200 m grid. The temperature retrievals were processed by the University Corporation for Atmospheric Research (UCAR), and obtained from the Web site http://www.cosmic.ucar.edu/.

2.3. ERA40 Reanalysis

[11] The European Centre for Medium Range Weather Forecasts (ECMWF) has produced a global reanalysis for the period 1957–2002 [*Uppala et al.*, 2005]. We use the analysis data on 60-model levels, with a resulting vertical resolution of ~1 km over the altitude range near the tropopause. We use the analysis temperature and wind fields, and calculate potential vorticity (PV) according to standard methods [e.g. *Andrews et al.*, 1987], with results in so-called PV units (10^6 K m^2 kg^{-1} s^{-1}). We use a series of PV isolines (PV = 1–4) to indicate the approximate location of the dynamical tropopause [e.g. *Hoerling et al.*, 1991].

[12] Thermal tropopauses are calculated from the ERA40 data according to the lapse rate definitions above, with the following modification. For defining a second tropopause, WMO criterion (b) is modified to use a 2 K/km value (rather than 3 K/km), based on the empirical finding that this produces results in better agreement with radiosonde and GPS data (which have higher vertical resolution). Details of this aspect of data analysis are discussed in Appendix.

2.4. Ozone

[13] We include analysis of ozone variability associated with double tropopause behavior, based on balloon (ozonesonde) and satellite observations. There are several ozonesonde stations over NH midlatitudes with relatively long observational records [e.g. *Logan et al.*, 1999], and these provide numerous observations of ozone profiles with both single and double tropopauses (identified using temperatures from radiosondes, which are included on the balloons with each ozonesonde). Results are shown here for several midlatitude stations, with data obtained from the World Ozone and Ultraviolet Radiation Data Center (WOUDC) web site (http://www.woudc.org/). We also use satellite ozone

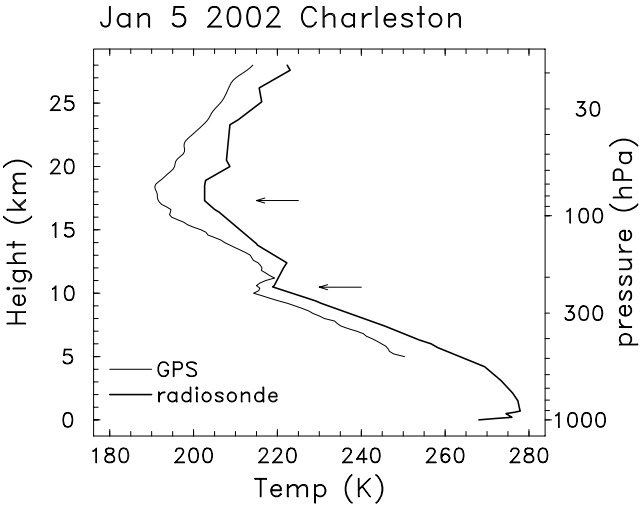

Figure 1. Vertical temperature profiles near Charleston on 5 January 2002, derived from radiosonde and GPS data. For clarity, the GPS profile is offset by 10 K from the radiosonde profile. The arrows denote the location of tropopauses defined by the temperature lapse rate criterion.

measurements from the Stratospheric Aerosol and Gas Experiment II (SAGE II) instrument [*McCormick et al.*, 1989]. These data are based on solar occultation measurements, with characteristic high vertical resolution and ability to resolve structure in the UTLS region [*Kar et al.*, 2002]. SAGE II data provide ozone profile measurements for altitudes above ~5–10 km (with a lower limit determined by cloud cover), with a vertical resolution of 0.5 km. The analyses here are based on SAGE II profile measurements during 2002–2004, used in conjunction with co-located (interpolated) ERA40 temperatures to determine tropopause structure.

3. Identification and Climatological Variability

3.1. Station Statistics and Synoptic Structure

[14] An example of a temperature profile where a double tropopause is identified is shown in Figure 1, where radiosonde data for 5 January 2002 from Charleston, South Carolina, USA (32 N, 280 E) are shown. Charleston is a typical subtropical station where frequent occurrences of double tropopauses are observed, and a long record of high-quality radiosonde data is available. The profile shows a tropopause identified near 10 km (associated with a temperature inversion above this level), and a second tropopause near 16 km. For comparison, Figure 1 also shows a GPS temperature profile near Charleston on this day, revealing a very similar vertical structure. The double tropopause structure seen in Figure 1 is a characteristic observed in over 70% of the profiles at Charleston during winter (as shown below).

[15] Of the three data sources, radiosonde and GPS data have the highest vertical resolution, and so best resolve double tropopauses. The ERA40 60-level data, with slight modifications to the tropopause definition (see Section 2a), are also able to resolve this behavior, and have the additional benefit of dynamically consistent three-dimensional meteorological fields to accompany the soundings. Figures 2 and 3 show aspects of the synoptic situation associated with the double tropopause profiles at Charleston seen in Figure 1, as derived from ERA40 data. Figure 2 shows a map identifying the locations of double tropopause occurrences (derived from temperature profiles at each grid point) for this particular day, together with the approximate location of the PV tropopause on the 200 hPa pressure surface (which is typically near the core of the jet). For this day (and for much of the NH winter) we identify a double tropopause over much of the NH midlatitudes, mainly on the poleward side of the PV tropopause at 200 hPa, spanning ~10–20 degrees latitude. Figure 3 shows vertical cross sections of the structure near Charleston (longitude 280 E); Figure 3a includes zonal winds, isentropes, PV isolines and identified tropopause positions, and Figure 3b shows the static stability structure together with the tropopause locations. These data illustrate the fact that the thermal tropopause has a characteristic discontinuous structure near the subtropical jet core, and that stability profiles exhibit a double tropopause over latitudes ~30–50 N (Charleston is near 32 N). Note that for this situation, the PV tropopause (identified by the PV = 1–4 isolines) does not exhibit a strongly folded structure.

[16] The static stability structure (Figure 3b) is quantified by the Brunt-Vaisala frequency squared (N^2), with enhanced stability (values $>2.10^{-4}$ s^{-2}) characteristic of stratospheric air [*Andrews et al.*, 1987]. As expected, tropopauses in Figure 3b are coincident with regions of enhanced vertical gradient in stability. The extension of the low latitude tropopause above LRT1 (over 30–50 N) corresponds to a region of relatively lower stability between LRT1 and LRT2, which appears continuous from lower latitudes. This structure is accentuated by a relative maximum in stability in a narrow layer above LRT1, which is associated with the temperature inversion above 10 km seen in Figure 1. We note that this structure is consistent with the tropopause inversion layer identified as a climatological feature in high-resolution radiosonde data by *Birner* [2006].

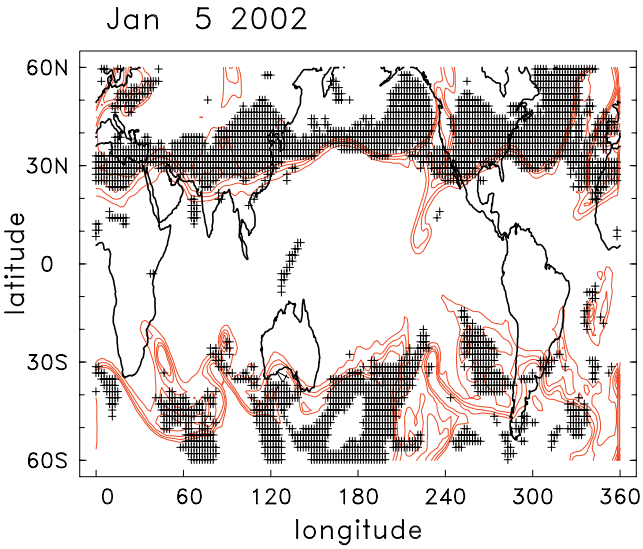

Figure 2. Locations of double tropopause occurrences (plus signs) derived from gridded ERA40 temperature data for 5 January 2002. The red lines show contours of PV = 1–4 at on the 200-hPa pressure level, denoting the approximate location of the dynamical tropopause at this level.

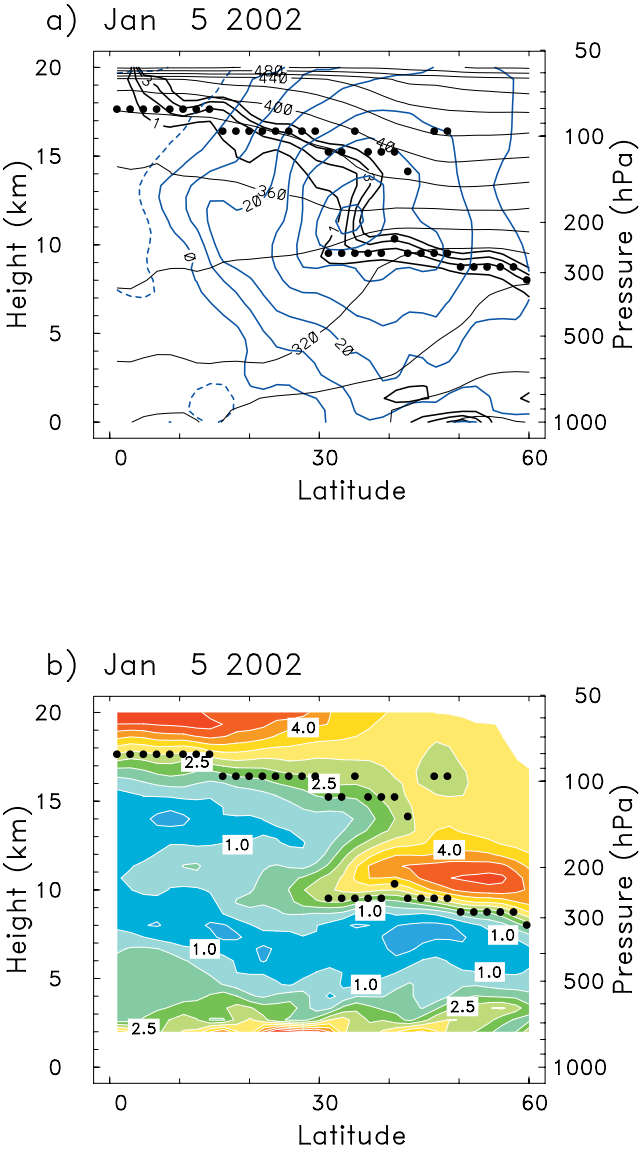

Figure 3. (a) Height-latitude cross section of dynamical structure at 280 E (near Charleston) derived from ERA40 data, including zonal winds (blue contours, m/s), isentropes (quasi-horizontal lines, contours at 20 K intervals), PV (heavy lines, contours of 1–4 PV units), and locations of the thermal tropopause (denoted by dots). (b) Corresponding static stability structure. Contours show Brunt-Vaisala frequency squared (N^2), with contour interval of 0.5 × 10^{-4} s^{-2}. Dots denote locations of the thermal tropopause (identical to (a)).

[17] Figures 4a and 4b show the January and July distributions of tropopause heights identified from Charleston radiosonde soundings during 1970–2004. These plots show the distribution for LRT1 with shaded data bins, and occurrences of higher tropopauses with unshaded data bins. The statistics for January show an overall bimodal distribution, with maxima near 11–12 km (primarily associated with LRT1) and 16–17 km (mainly LRT2). There are a relatively small number of profiles in January with LRT1 near 16 km, and these represent cases where the sounding is tropical in character. July statistics in Figure 4b show a single maximum (primarily LRT1) centered near 15 km, reflecting the fact that double tropopauses are not often observed during the summer. Figures 4c and 4d show similar statistics derived from GPS data for soundings within 300 km of Charleston during 2001–2005. These data show similar statistics to the longer radiosonde record, and we find similar agreement at many other radiosonde stations (not shown here). One small difference that occurs between GPS and radiosonde statistics is that there are slightly more January cases where tropical profiles are identified (i.e. LRT1 > 15 km) in the GPS statistics (cf. Figures 4a to 4c). Comparison of co-located soundings shows that this can occur because a small feature identified as an LRT1 below 14 km in a radiosonde profile may not satisfy the WMO criterion in the GPS profile; this difference is likely related to the different vertical and/or horizontal resolution of the respective measurements. This difference has a minor influence on double tropopause statistics, which are slightly less frequently found in the GPS data.

[18] Figure 5 shows the seasonal variation of the number of soundings with multiple tropopauses at Charleston, comparing radiosonde data (1970–2004) and GPS statistics (2001–2005). Results are similar in both data sets, showing multiple tropopauses occur for approximately 60–80% of the soundings during winter-spring (December–April). Very few multiple tropopauses (~10%) are observed during summer (June–September). The statistics in Figure 5 include separate results for profiles with two and three tropopause occurrences, and during winter three tropopauses are identified for approximately 10–20% of the profiles. These are probably the result of large amplitude waves influencing the stability profile, rather than a distinct phenomenon.

[19] The seasonal variation of mean tropopause heights for LRT1 and LRT2 at Charleston are shown in Figure 6; note that we do not define a mean for LRT2 during summer (June–September), when the occurrence frequency is below 20% (Figure 5). The mean altitude of LRT1 exhibits a strong annual cycle, varying from near 12 km in winter to near 15 km in summer, which is typical of NH midlatitudes [*Seidel and Randel*, 2006]. The mean location of the upper tropopause (LRT2) is near 16 km for all months, similar to the tropical tropopause. The fact that the altitude of LRT1 in summer approaches the mean altitude of LRT2 may be part of the reason why LRT2 is not detectable in summer.

[20] The double tropopause behavior is also observed at high latitudes, but somewhat less frequently than in the subtropics. Figure 7a shows tropopause height statistics in January for Annette Island, Alaska, USA (55 N, 230 E), revealing a bimodal distribution related to multiple tropopauses. These occur in over 40% of the soundings during winter (Figure 7b). The morphology of these events is similar to the situation seen in Figure 3, with the upper tropopause (near 16 km) extending more or less continuously from the tropics.

[21] Some statistics for a Southern Hemisphere station (Adelaide, 34 S, 190 E) are shown in Figure 8. As in the NH, a bimodal tropopause height distribution is observed during winter (July, Figure 8a), and multiple tropopauses are observed approximately 50% of the time (Figure 8b). The summer minimum in multiple tropopause occurrences is less pronounced in the SH, and the overall seasonal cycle is weaker than that observed in the NH (c.f. Figures 5 and 8b).

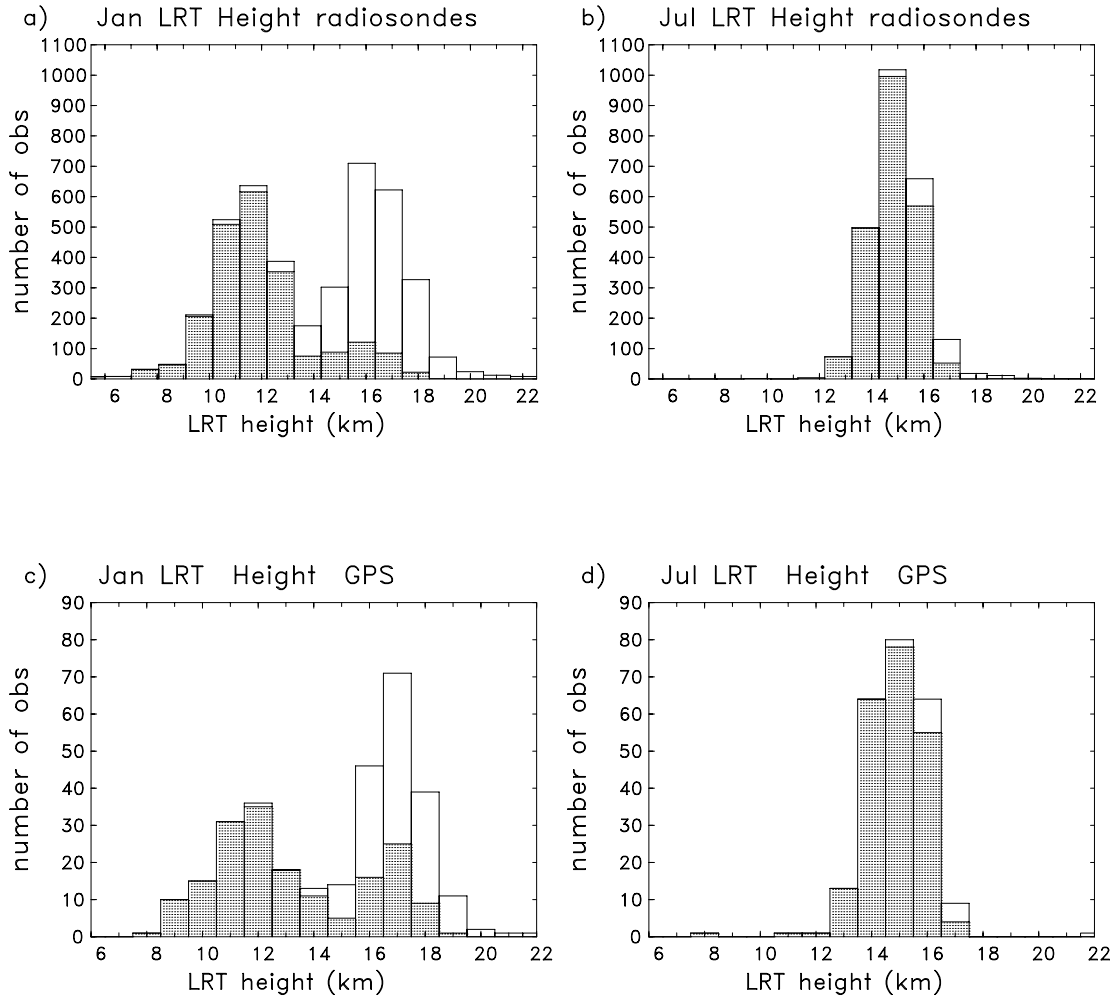

Figure 4. Tropopause height distributions derived from radiosonde measurements at Charleston for 1970–2004, for statistics during January (a) and July (b). Shaded bins show statistics for LRT1, and unshaded bins show those for higher level tropopauses. Panels (c–d) show corresponding results derived from GPS measurements near Charleston during 2001–2005.

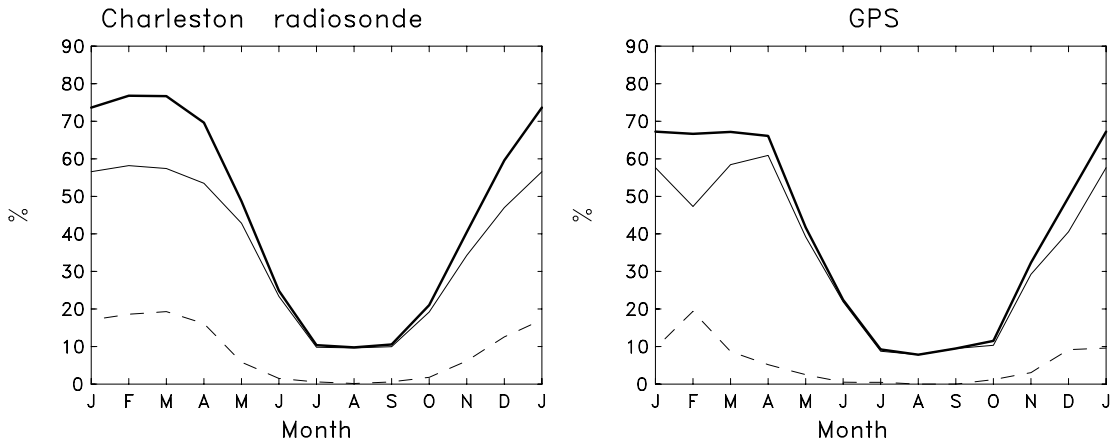

Figure 5. Seasonal cycle of multiple tropopause occurrences at Charleston, derived from radiosondes for 1970–2004 (a) and GPS data for 2001–2005 (b). Heavy line denotes the occurrence frequency for more than one tropopause; this is composed of occurrences with two (light solid) and three (dashed) tropopauses in individual soundings.

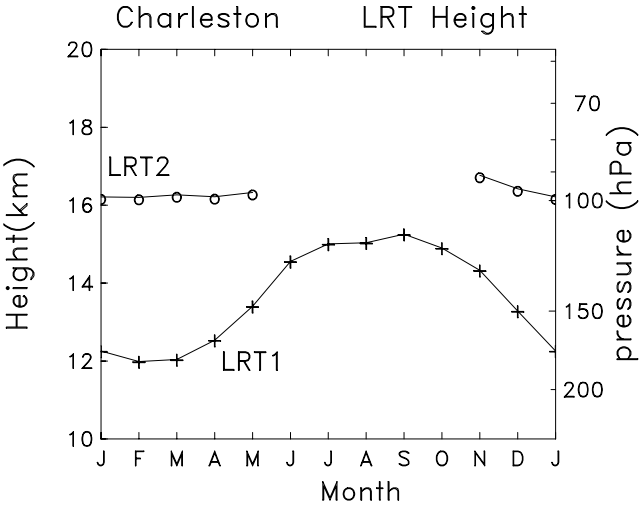

Figure 6. Seasonal cycle of mean tropopause heights at Charleston, derived from radiosonde data over 1970–2004. Results are shown for LRT1 and LRT2; the latter is not included during summer, when occurrence frequency is below 20%.

The mean altitude of LRT1 (Figure 8c) undergoes a seasonal variation between ~11 km (winter) and ~15 km (summer), similar to the NH (Figure 6). The mean altitude of LRT2 is near 16 km, with a relatively weak seasonal variation (higher during SH summer) that is similar to the tropical tropopause [*Seidel et al.*, 2001].

3.2. Global Statistics From GPS Data

[22] The good agreement found between tropopause statistics derived from radiosondes and GPS data suggests that the latter may be useful to quantify the global space-time variability of double tropopause behavior. The latitude-longitude structure of double tropopause occurrence frequency from GPS data is shown in Figure 9, for NH winter (December–February, DJF) and NH summer (June–August, JJA). These are derived from GPS observations in 10 degree latitude by 30 degree longitude bins. The double tropopause climatology for DJF (Figure 9a) shows maxima of ~50–60% over NH midlatitudes, and values of ~30% over SH midlatitudes. Small frequencies are observed in the tropics (~10%), and the few cases that occur there are primarily associated with large amplitude wave structures in the lower stratosphere, that produce secondary tropopauses above 17 km [e.g. large amplitude Kelvin waves, *Randel and Wu*, 2005]. There is relatively weak zonal structure to the NH midlatitude occurrence frequency in Figure 9a (percentages range from ~45 to 60%), and no clear association with the longitudinal maximum observed in storm tracks statistics [such as eddy variances, *Peixoto and Oort*, 1992, or tropopause fold statistics, *Sprenger et al.*, 2003]. During SH winter (JJA, Figure 9b) there is a relative maximum occurrence frequency of ~40% over SH midlatitudes, also with weak zonal structure. Figure 9b also shows a localized maximum in double tropopause occurrence (over 40%) in the NH, near the region of the south Asian summer monsoon anticyclone.

[23] The synoptic situation associated with double tropopauses near the Asian monsoon is shown for a particular day (July 5, 2002) in Figure 10. Here the ERA40 data are used to identify double tropopause locations (Figure 10a) and show the related dynamical structure in the monsoon region near 90 E (Figure 10b). The Asian monsoon circulation includes a strong anticyclonic flow in the UTLS region, with a relatively high (tropical) tropopause extending to ~30 N [*Highwood and Hoskins*, 1998; *Randel and Park*, 2006]. Double tropopauses occur on the poleward flank of the anticyclonic circulation (the region of westerly zonal winds), where the tropopause near 16 km extends poleward to approximately 60 N (Figure 10b). The overall dynamical structure is similar to that seen in NH winter midlatitudes (Figure 3a), and the stability structure (not shown) is similar to that in Figure 3b. Note also the relatively continuous band of double tropopauses observed over SH (winter) midlatitudes in Figure 10a, similar to the NH winter structure seen in Figure 2.

[24] It is well known that the altitude of LRT1 in the extratropics is strongly dependent on the local synoptic situation, with cyclonic UTLS circulation associated with

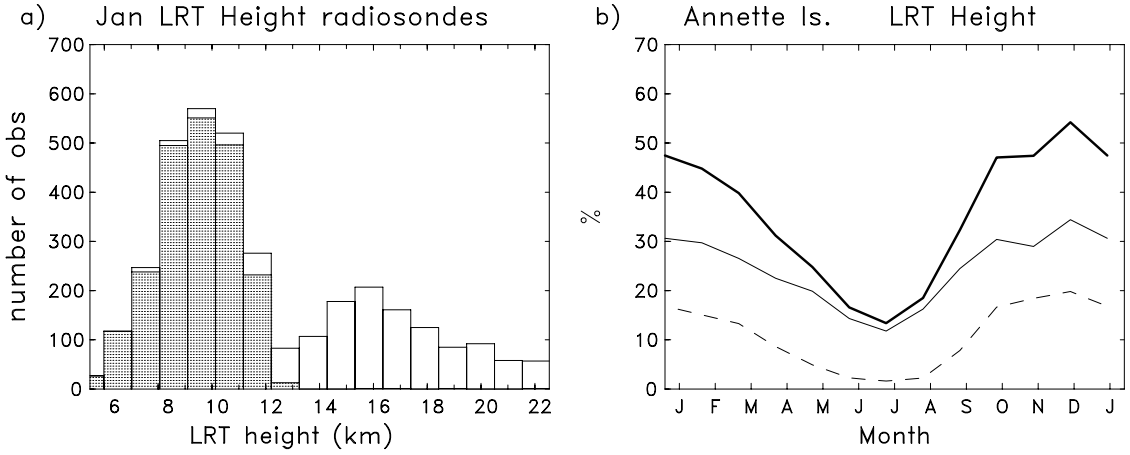

Figure 7. (a) Tropopause height distribution at Annette Island, Alaska (55 N) during January, derived from radiosonde statistics. Shaded bins are for LRT1. (b) Seasonal variation of multiple tropopause occurrence frequency at Annette Island. Details are the same as Figures 4 and 5.

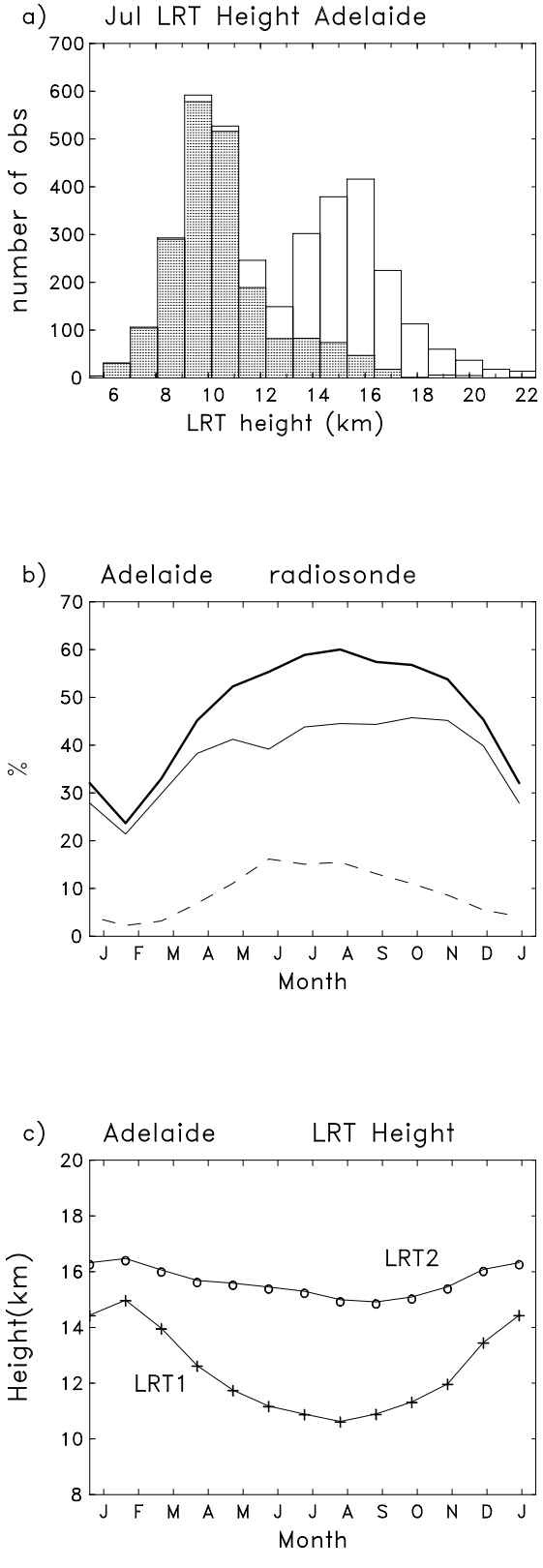

Figure 8. Tropopause height statistics at Adelaide, Australia (34 S), derived from radiosondes covering 1974–2004. Shaded bins are for LRT1. (a) Tropopause height distribution during winter (July). (b) Seasonal variation of multiple tropopause occurrence frequency (details are the same as Figure 4). (c) Seasonal variation of tropopause heights for LRT1 and LRT2.

a relatively low tropopause (in the NH), and anticyclonic circulation with a high tropopause [e.g. *Hoskins et al.*, 1985; *Wirth*, 2001]. To determine if double tropopause occurrences have some relationship with circulation, we have evaluated the upper troposphere (200 hPa) relative vorticity (estimated from the ERA40 reanalyses) co-located with each GPS sounding, and then calculated tropopause statistics as a function of relative vorticity. Figure 11 shows results from NH winter, based on data sampled during DJF over 30–60 N (a total of 4021 soundings). The vorticity distribution exhibits a skew toward cyclonic vorticity anomalies. The altitude of LRT1 shows a monotonic change from relatively low tropopause (near 9 km) for cyclonic circulation, to a higher tropopause (~12 km) for anticy-

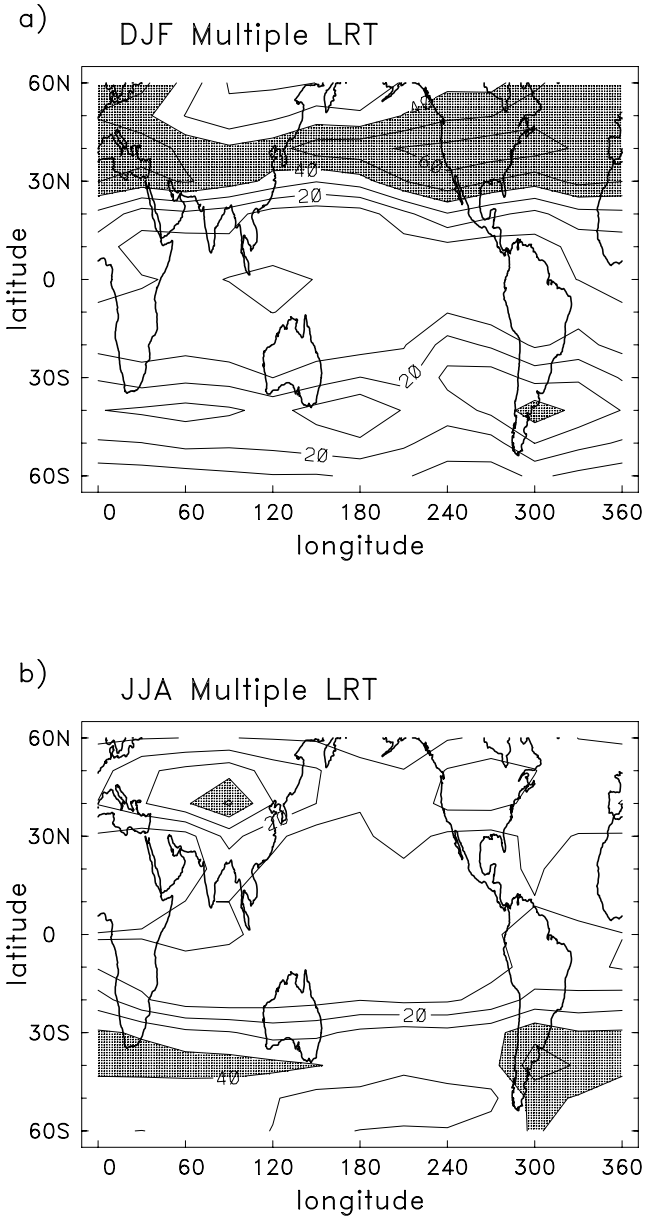

Figure 9. Climatological frequency of occurrence (%) of double tropopauses derived from GPS measurements during 2001–2004, for DJF (a) and JJA (b). Contour interval is 10%, with values above 40% shaded.

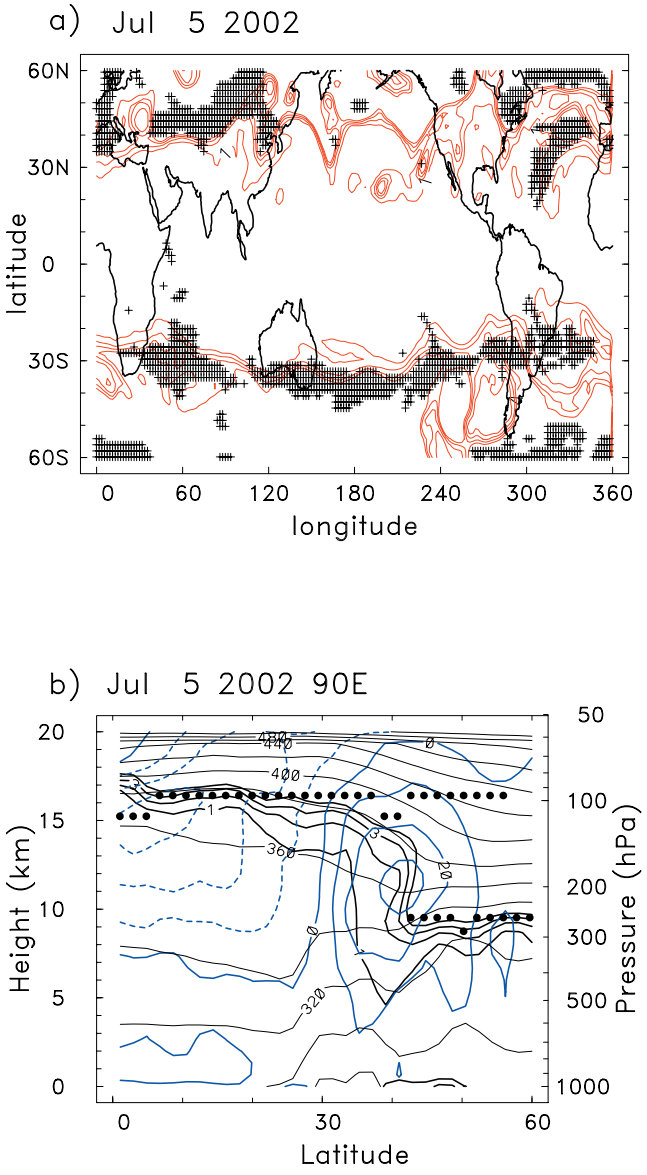

Figure 10. (a) Locations of double tropopause occurrences (plus signs) derived from gridded ERA40 temperature data for 5 July 2002. The red lines show contours of PV = 1–4 at on the 200 hPa pressure level, denoting the approximate location of the dynamical tropopause at this level. (b) Height–latitude cross section of dynamical structure at 90 E (over the Asian monsoon region) derived from ERA40 data, including zonal winds (blue contours, m/s), isentropes (quasi-horizontal lines, contours at 20 K intervals), PV (heavy lines, contours of 1–4 PV units), and locations of the thermal tropopause (denoted by dots).

clonic circulation [as expected, e.g. *Hoskins et al.*, 1985]. The altitude of LRT2 shows a similar but weaker dependence on circulation, with only ~1 km difference between cyclonic and anticyclonic flow. However, the frequency of occurrence for multiple tropopauses (top curve in Figure 11) exhibits a strong relationship to circulation, with the most intense cyclonic flows having a substantially higher fraction of double tropopauses (above 80%), compared to weak or anticyclonic flows (~50%). Analogous statistics derived for SH observations (not shown here) exhibit very similar dependence on vorticity. Thus strongly cyclonic circulations in midlatitudes are much more likely to exhibit a double tropopause structure, in conjunction with a lower LRT1, than weak or anticyclonic circulations. Note that while double tropopauses tend to occur on the poleward flank of the subtropical jet (Figures 2 and 3), the relative vorticity associated with latitudinal wind shear in this region is typically less than 10^{-4} s^{-1} (1 vorticity bin in Figure 11). Thus the dependence on local circulation in Figure 11 acts as a (strong) modulation of the general occurrence on the poleward jet flank.

[25] Figure 12 shows the climatological altitude of LRT1 and LRT2 for statistics during DJF and JJA, derived from GPS data. Here the altitude of LRT2 is calculated only for locations where the occurrence frequency of double tropopauses exceeds 20% (from Figure 9); thus the NH JJA statistics are based only on the Asian monsoon region. Statistics for LRT1 show the well-known latitude and

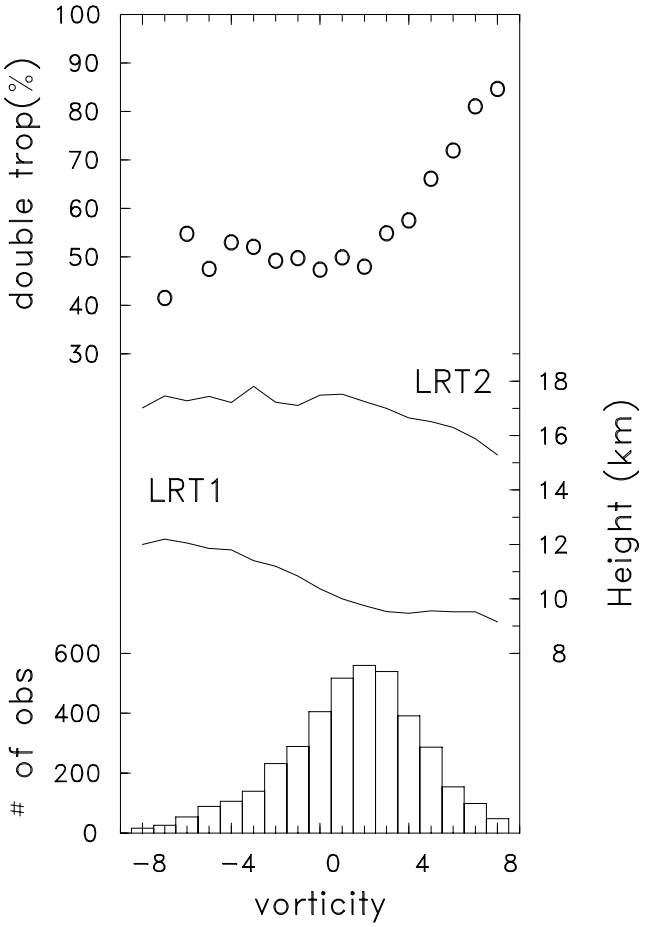

Figure 11. Distribution of relative vorticity at 200 hPa (histogram at bottom; units are 10^{-4} s^{-1}), along with tropopause statistics derived from GPS data, for NH winter (December–February) data over 30–60 N. Relative vorticity is derived from ERA40 data coincident with the GPS measurements, and tropopause statistics are derived for each vorticity bin; results are shown for the average height of LRT1 and LRT2, and the fraction of profiles with double tropopauses.

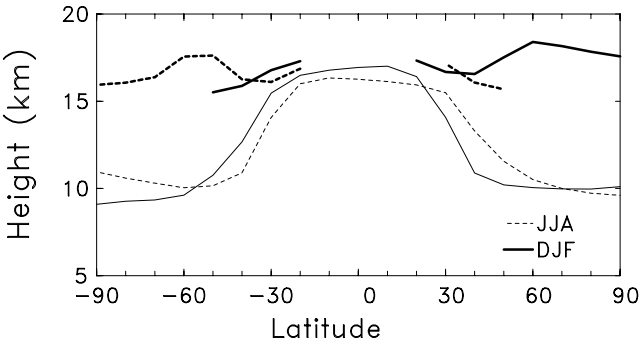

Figure 12. Latitudinal profile of the zonal average mean altitude of LRT1 (light curves) and LRT2 (heavy curves), based on GPS statistics during DJF and JJA. Results for LRT2 are derived only for locations where the occurrence frequency is more than 20%.

seasonal variations [e.g. *Hoinka*, 1998]. LRT2 shows a mean altitude of 16–18 km over the entire extratropics of both hemispheres, with a symmetric latitudinal structure between the NH and SH. *Thuburn and Craig* [2002] demonstrated that radiative processes are a key factor determining the altitude of the tropical tropopause; the similarity in altitude between LRT2 and the tropical tropopause suggests that radiative processes are also important for maintaining LRT2. While our results have not focused on polar regions, the GPS statistics show that an LRT2 can often occur over polar latitudes in winter. We note that the results in Figure 12 are substantially different from the analysis of GPS data by *Schmidt et al.* [2006], as they calculate a climatological LRT2 that more closely follows the latitudinal structure of LRT1 (their Figure 1); the reason for this discrepancy is unknown.

4. Double Tropopauses and Ozone Behavior

[26] Ozone is a long-lived tracer in the UTLS region with strong gradients between the troposphere and stratosphere, and it provides a useful diagnostic for transport behavior. We have examined ozone profiles from balloon and satellite measurements to search for systematic behavior associated with double tropopauses. Balloon-borne ozonesonde measurements always include a radiosonde temperature profile, so that identification of tropopause structure is straightforward. Figure 13 shows ozone profiles for averages of soundings with a single or double tropopauses, for NH winter-spring measurements at Boulder, Colorado (40 N), Payerne, Switzerland (46 N) and Churchill, Canada (59 N). These stations all have relatively long records with data covering ~20 years, so that there are numerous soundings with both single and double tropopauses (the total number of winter-spring ozonesonde profiles is 390 for Boulder, with 69% having double tropopauses; the corresponding values are 1756 (45%) for Payerne and 402 (20%) for Churchill). The separation of single versus double tropopause profiles exerts a strong influence on the ozone statistics in Figure 13, with double tropopause profiles exhibiting systematically less ozone in the lower stratosphere (over altitudes ~12–

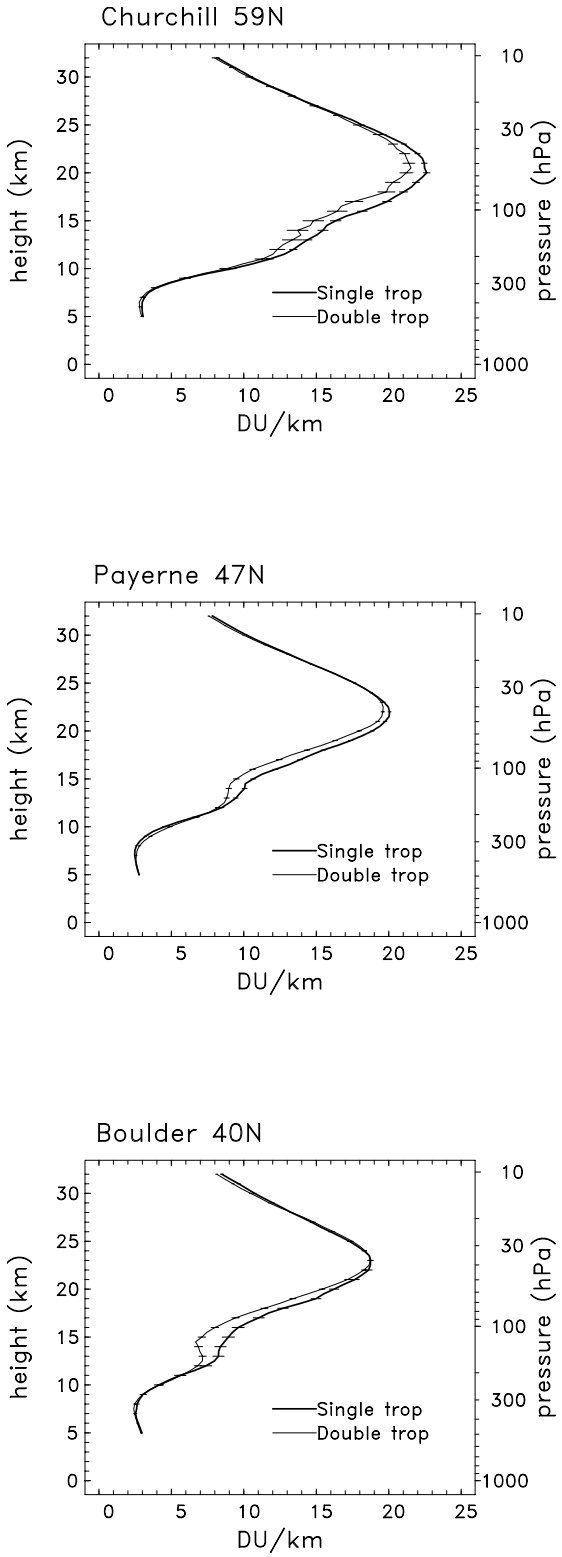

Figure 13. Vertical profiles of ozone observed by ozonesondes at Boulder, Payerne and Churchill (bottom to top), segregated according to if the temperature profiles exhibit a single or double tropopause (heavy and light lines in each panel). Horizontal bars denote the standard deviation of the means within each group.

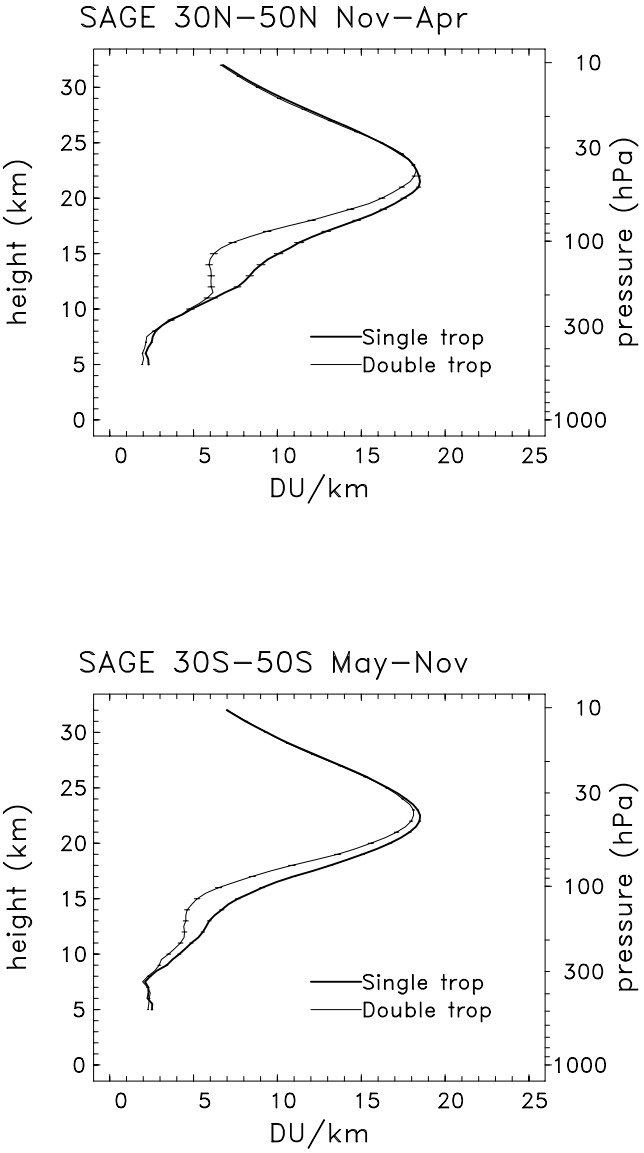

Figure 14. Vertical profiles of ozone observations from SAGE II during 2002–2004, segregated according to profiles with single and double tropopauses (heavy and light lines). Statistics are calculated from observations over 30–50 N during November–April (top) and over 30–50 S during May–November (bottom). Horizontal bars denote the standard deviations of the means within each group.

22 km). Notably, this behavior is observed even for the high latitude measurements at Churchill (59 N).

[27] Figure 14 shows similar ozone statistics derived from SAGE II satellite measurements during 2002–2004, for observations over both hemispheres (1068 profiles during November–April in the NH, and 1167 profiles for May–November in the SH). Here ERA40 temperature data coincident with each SAGE II profile are used to determine single versus multiple tropopause profiles. The results in Figure 14 are very similar to the ozonesonde averages, showing lower ozone amounts in the lower stratosphere for profiles with double tropopauses. The vertical extent of the region with significant ozone differences (~12–22 km) is very similar between NH and SH statistics in Figure 14, and also consistent with the ozonesonde results (Figure 13). Overall, the ozone measurements show systematic reductions in lower stratospheric ozone associated with double tropopause occurrences. Given the background latitudinal structure of ozone in the UTLS region (lower ozone in the tropics, and higher ozone at high latitudes), these results suggest that double tropopause occurrences in midlatitudes correspond to situations with enhanced transport from the tropics over the altitude region ~12–22 km (namely, above the core of the subtropical jet, as seen in Figure 3a). We note that *Hudson et al.* [2003] have demonstrated relationships between column and profile ozone and tropopause height (LRT1), which they discuss in terms of climate regimes; the analyses here show that the occurrence of a second tropopause (LRT2) is also a highly relevant factor for ozone.

5. Long-Term Changes in Double Tropopause Occurrence Statistics

[28] As we have shown, double tropopauses are found near the subtropical jet, and LRT2 has characteristics of the tropical LRT. These features suggest an interpretation of the location of frequent double tropopauses as a region of transition between the tropical and extratropical troposphere. Several investigators have suggested that long-term variations may exist in strength and/or location of the subtropical jets. For example, *Chang and Fu* [2002] suggest a decadal-scale increase in storm track intensity over much of the NH between the late 1960s and 1990s. Also, *Leroy et al.* [2006] have shown that poleward migration of the subtropical jets in both hemispheres is a signature of anthropogenic climate change in global climate model projections, and observed midlatitude temperature trends are consistent with this behavior [*Fu et al. 2006*]. These studies motivate examination of long-term changes in double tropopause frequency, possibly associated with changes in jet structure.

[29] We examined radiosonde data from a 100-station global network [*Seidel and Randel*, 2006] to search for trends in double tropopause frequency from the late 1950's through 2005. We found upward trends in the frequency of occurrence of double tropopauses at most stations, for the full period and for most subperiods. However, there is a strong possibility that these trends could be artifacts of long-term changes in the vertical resolution of the sounding data. During 1965–2005, the upper level of soundings increased at most stations, and the number of reported data levels increased at all stations. Part of the increase in number of levels is simply due to increased altitude of the soundings; however, we also find an increase of ~2–10 levels/decade in the 700–50 hPa layer for a majority of stations. This increased resolution is likely due to technological improvements in balloons and in the capability of ground stations to archive more data per sounding with the gradual introduction of automated recording systems and of computers with increased storage capacity. It is likely that this increase in vertical resolution of the soundings over time could substantially impact the likelihood of finding an LRT2. We thus believe that systematic changes in data resolution pose a severe constraint on the ability to detect

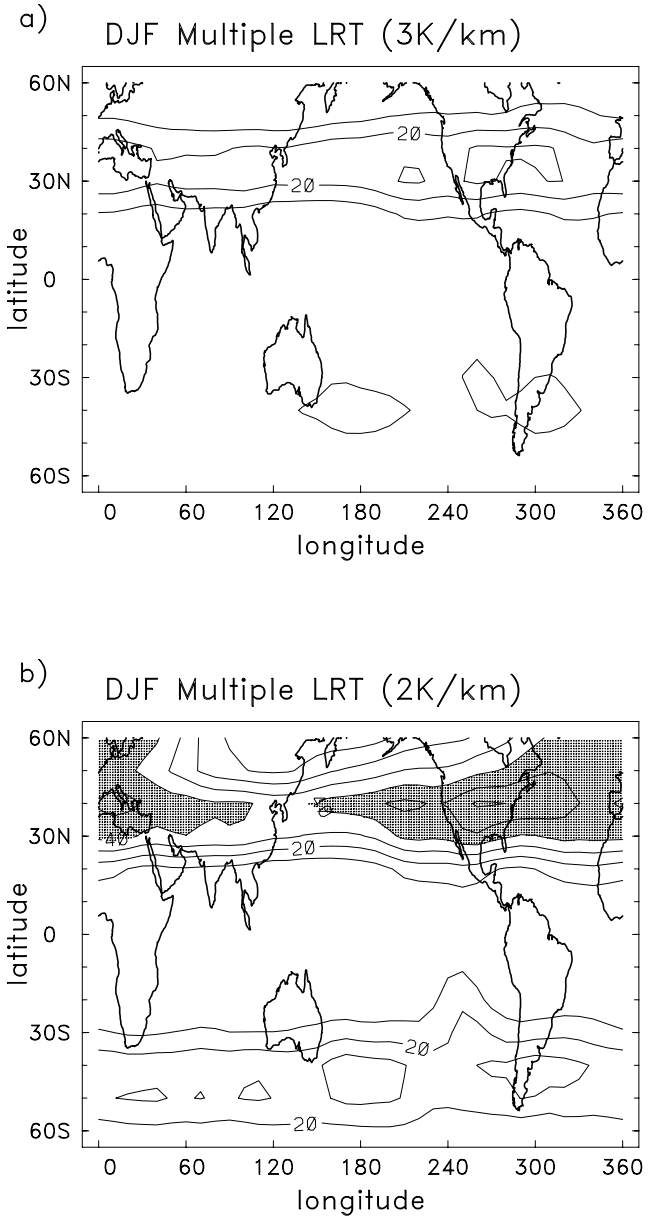

Figure A1. Climatological frequency of occurrence (%) of double tropopauses during DJF, derived from ERA40 data. Results in (a) are derived from the WMO definition of the second tropopause (Section 2a), while results in (b) use a slightly modified criterion based on a lapse rate of 2K/km above the first tropopause. Contours are the same as in Figure 9.

true trends in LRT2 occurrence frequency, and further examination of long-term trends is not pursued here.

6. Summary and Discussion

[30] This work has focused on describing the observational characteristics of double tropopauses, including their thermal and dynamical structure, global frequency of occurrence, and relation to ozone behavior. Double tropopauses occur frequently over midlatitude regions of both hemispheres. They are associated with a characteristic break in the thermal tropopause near the subtropical jet, where the low latitude (tropical) tropopause extends to higher latitudes, overlying the lower tropopause. This observed structure suggests that the latitude band of frequent double tropopauses behaves as a transition region between the tropics and extratropics. The observed behavior of ozone supports this interpretation, as ozone values in double tropopause situations are midway between those in the tropical upper troposphere (low) and extratropical lower stratosphere (high).

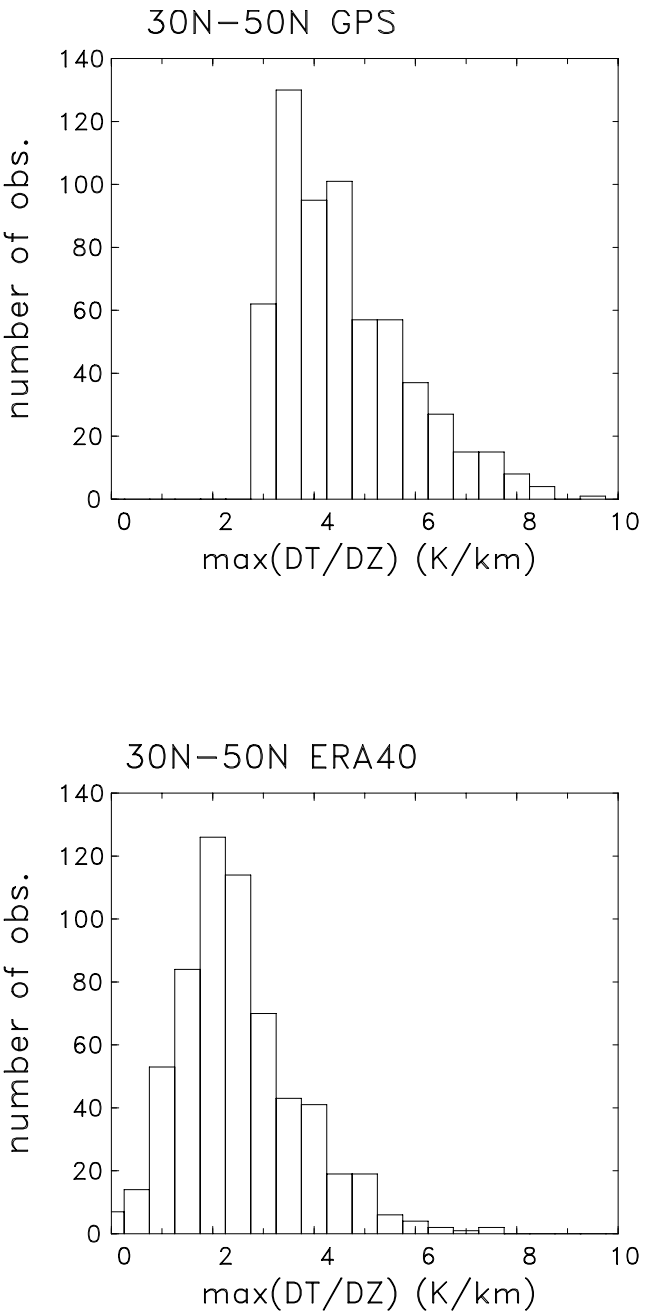

Figure A2. (a) Distribution of the maximum lapse rate above LRT1 for profiles with a double tropopause, for GPS data sampled over the 30–50 N during DJF. (b) Distribution of the maximum lapse rate for the same profiles as in (a), but calculated using ERA40 data (co-located with the GPS profiles).

[31] A key feature of having a second tropopause (LRT2) is that the lapse rate above LRT1 increases to some value characteristic of the troposphere (greater than 3 K/km, according to the WMO definition). The cross section shown in Figure 3b, which is typical, shows that this region of tropospheric-like stability above LRT1 is contiguous with low stability in the tropical upper troposphere. This structure suggests that a secondary tropopause is often associated with the poleward transport of tropical tropospheric air in the region above the subtropical jet core (Figure 3b). This interpretation is consistent with lower ozone above LRT1 in double tropopause situations; that is, the advected air in this region has both low stability and low ozone, characteristic of the tropical upper troposphere. The mechanism of systematic poleward transport in the region above the jet is unclear, but may include contributions from both the thermally direct (clockwise in Figure 3a) secondary circulation associated with developing baroclinic waves [e.g. *Keyser and Shapiro*, 1986, Figure 28], and quasi-horizontal mixing along isentropes above the jet core [e.g. *Haynes and Shuckburgh*, 2000]. Whatever the cause, the ozone observations (Figures 13 and 14) suggest that it is a relatively deep circulation extending into the lower stratosphere ($\sim$20 km).

[32] As a note, the specific frequency of occurrence for double tropopauses is in fact dependent on the value of the lapse rate criterion chosen above LRT1 (3 K/km for the WMO criterion), with a systematic increase of occurrence for lower thresholds. For example, based on GPS data, the maximum NH DJF occurrence over North America (60% in Figure 9a) increases to over 80% if a 2 K/km threshold is used, and decreases to $\sim$30% if a 4 K/km value is used (although the spatial patterns are unchanged). Thus the specific percentage values for double tropopause occurrences may be less important than the identification of some tropospheric-like stability above LRT1.

[33] Double tropopauses occur most frequently above strong cyclonic circulation systems. This is probably due to the balanced dynamical structure associated with cyclonic UTLS circulation, wherein the stability in the lower stratosphere (above LRT1) is reduced; this effect can enhance low stability in this region arising from transport (discussed above), resulting in a high frequency of double tropopause occurrences. A calculation of the maximum lapse rate between LRT1 and LRT2 as a function of vorticity (as in Figure 11) confirms this dependence, revealing stronger lapse rates for more intense cyclonic circulations (not shown here). The frequent occurrence of double tropopauses during NH winter (Figure 9) may be due to the stronger overall atmospheric circulation at this time (and associated distribution of stronger cyclonic circulation systems). Similarly, the lack of double tropopauses over the majority of the NH during summer may be due to the overall weak circulation at this time (away from the Asian monsoon region), together with the fact that summer LRT1 are already relatively high ($\sim$15 km).

[34] Although double tropopauses appear as a climatological feature in midlatitudes, with strong links to local circulation intensity (Figure 11), the spatial patterns of occurrence frequency (Figure 9) do not show strong zonal structure, such as maxima in the storm track regions. This makes double tropopause statistics somewhat different from tropopause fold behavior, which exhibit clear maxima in storm track regions [*Elbern et al.*, 1998; *Wernli and Bourqui*, 2002; *Sprenger et al.*, 2003]. Neither is there a strong relationship between double tropopauses and occurrences of quasi-horizontal Rossby wave breaking events in the UTLS region [*Postel and Hitchman*, 1999], as the latter are most frequent during summer.

Appendix A: Tropopause Statistics From ERA40 Data

[35] Derivation of double tropopause statistics from the 60-level ERA40 data, using the standard WMO definition (Section 2a), gives substantially fewer occurrences compared to values derived from radiosondes or GPS data. For example, Figure A1a shows the climatological frequency of occurrence in ERA40 data for DJF, showing about half the magnitude of the GPS climatology in Figure 9a. This difference is fundamentally due to the strength of the lapse rates above LRT1 derived from the ERA40 data, and the WMO criterion (3 K/km, item (b) in Section 2a). Figure A2a shows a distribution of the maximum lapse rate in double tropopause situations as evaluated with GPS data over $30^\circ - 50^\circ$ N during DJF (note there are only values greater than 3 K/km). Figure A2b shows the same statistics derived from ERA40 data co-located with each of the individual GPS soundings, with a systematic shift in the distribution to smaller maximum lapse rates (probably associated with a lack of vertical resolution in the ERA40 data). In particular, about half of the ERA40 profiles have a maximum lapse rate less than 3 K/km, which results in about half as many identified double tropopauses (cf. Figures A1a and 9a). If the criterion is modified to 2 K/km for the ERA40 data, then the double tropopause statistics (Figure A1b) are similar to results from GPS data. A similar agreement is seen comparing statistics throughout the year, and for specific vertical profiles. Hence it seems reasonable to use the reduced (2 K/km) constraint when analyzing the ERA40 data for identifying double tropopause occurrences (and this is what was used in Figures 2, 3 and 10).

[36] **Acknowledgments.** We thank Fei Wu at NCAR for much of the data analysis presented here. We also thank several colleagues for discussions during the course of this work and comments on the manuscript, including Jim Angell, Ken Bowman, Chris Davis, Dan Kirk-Davidoff, John Nielsen-Gammon, Rolando Garcia, Peter Haynes, and Lorenzo Polvani. We appreciate constructive reviews from Thomas Birner and two anonymous referees. This work was partially supported by the NASA ACMAP Program. The National Center for Atmospheric Research is operated by the University Corporation for Atmospheric Research, under sponsorship of the National Science Foundation.

References

Andrews, D. G., J. R. Holton, and C. B. Leovy (1987), *Middle Atmosphere Dynamics*, Academic Press, 489 pp.

Bithel, M., L. J. Gray, and B. D. Cox (1999), A three-dimensional view of the evolution of midlatitude stratospheric intrusions, *J. Atmos. Sci.*, *56*, 673–688.

Birner, T. (2006), Fine-scale structure of the extratropical tropopause region, *J. Geophys. Res.*, *111*, D04104, doi:10.1029/2005JD006301.

Bischoff, S. A., P. O. Canziani, and A. E. Yuchechen (2007), The tropopause at southern extratropical latitudes: Argentine operational rawinsonde climatology, *Int. J. Climatology*, *27*, 189–209, doi:10.1002/joc.1385.

Bjerknes, J., and E. Palmen (1937), Investigation of selected European cyclones by means of serial ascents. Geofis. Publ. 12, 62pp. A. Meteorol. Soc., Boston, MA.

Browell, E. V., E. F. Danielsen, S. Ismail, G. L. Gregory, and S. M. Beck (1987), Tropopause fold structure determined from airborne lidar and in situ measurements, *J. Geophys. Res.*, *92*, 2112–2120.

Chang, E. K. M., and Y. Fu (2002), Interdecadal variations in Northern Hemisphere winter storm track intensity, *J. Climate*, *15*, 642–658.

Durre, I., R. S. Vose, and D. B. Wuertz (2006), Overview of the Integrated Global Radiosonde Archive, *J. Climate*, *19*, 53–68.

Elbern, H., et al. (1998), A climatology of tropopause folds by global analyses, *Theor. Appl. Climatol.*, *59*, 181–200.

Fu, Q., C. M. Johanson, J. M. Wallace, and T. Reichler (2006), Enhanced mid-latitude tropospheric warming in satellite measurements, *Science*, *312*, 1179, doi: 10.1126/science.1125566.

Hajj, G. A., et al. (2004), CHAMP and SAC-C atmospheric occultation results and intercomparisons, *J. Geophys. Res.*, *109*, D06109, doi:10.1029/2003JD003909.

Haynes, P., J. Scinocca, and M. Greenslade (2001), Formation and maintenance of the extratropical tropopause by baroclinic eddies, *Geophys. Res. Lett.*, *28*(22), 4179–4182.

Haynes, P., and E. Shuckburgh (2000), Effective diffusivity as a diagnostic of atmospheric transport 2. Troposphere and lower stratosphere, *J. Geophys. Res.*, *105*(D18), 22,795–22,810.

Held, I. (1982), On the height of the tropopause and the static stability of the troposphere, *J. Atmos. Sci.*, *39*, 412–417.

Highwood, E. J., and B. J. Hoskins (1998), The tropical tropopause, *Q.J.R. Meteorol. Soc.*, *124*, 1579–1604.

Hoerling, M. P., T. K. Schaack, and A. J. Lenzen (1991), Global objective tropopause analysis, *Mon. Wea. Rev.*, *126*, 3303–3325.

Hoinka, K. P. (1998), Statistics of the global tropopause pressure, *Mon. Wea. Rev.*, *126*, 3303–3325.

Holton, J. R., et al. (1995), Stratosphere-troposphere exchange, *Rev. Geophys.*, *33*, 403–439.

Hoskins, B. J., M. E. McIntyre, and A. W. Robertson (1985), On the use and significance of isentropic potential vorticity maps, *Quart. J. Roy. Meteor. Soc.*, *111*, 877–946.

Hudson, R. D., A. D. Frolov, M. F. Andrade, and M. B. Follette (2003), The total ozone field separated into meteorological regimes, Part I. Defining the regimes, *J. Atmos. Sci.*, *60*, 1669–1677.

Kar, J., C. R. Trepte, L. W. Thomason, and J. M. Zawodny (2002), Observations of layers in ozone vertical profiles from SAGE II (v 6.0) measurements, *Geophys. Res. Lett.*, *29*(10), 1433, doi:10.1029/2001GL014230.

Keyser, D., and M. A. Shapiro (1986), A review of the structure and dynamics of upper-level frontal zones, *Mon. Wea. Rev.*, *114*, 452–499.

Kochanski, A. (1955), Cross sections of the mean zonal flow and temperature along 80, *W. J. Meteor.*, *12*, 95–106.

Kursinski, E. R., et al. (1996), Initial results of radio occultation observations of Earth's atmosphere using the Global Positioning System, *Science*, *271*, 1107–1110.

Leroy, S. S., J. G. Anderson, and J. A. Dykema (2006), Testing climate models using GPS radio occultation: A sensitivity analysis, *J. Geophys. Res.*, *111*, D17105, doi:10.1029/2005JD006145.

Logan, J. A., et al. (1999), Trends in the vertical distribution of ozone: A comparison of two analyses of ozonesonde data, *J. Geophys. Res.*, *104*(D21), 26,373–26,399.

McCormick, M. P., J. M. Zawodny, R. E. Viega, J. C. Larson, and P. H. Wang (1989), An overview of SAGE I and II ozone measurements, *Planet. Sp. Sci.*, *37*, 1567–1586.

Nielsen-Gammon, J. W. (2001), A visualization of the global dynamic tropopause, *Bull. Amer. Meteor. Soc.*, *82*, 1151–1168.

Pan, L. L., et al. (2004), Definitions and sharpness of the extratropical tropopause: A trace gas perspective, *J. Geophys. Res.*, *109*, D23103, doi:10.1029/2004JD004982.

Peixoto, J. P., and A. H. Oort (1992), *Physics of Climate*. American Institute of Physics.

Postel, G. A., and M. Hitchman (1999), A climatology of Rossby wave breaking along the subtropical tropopause, *J. Atmos. Sci.*, *56*, 359–373.

Randel, W. J., and F. Wu (2005), Kelvin wave variability near the equatorial tropopause observed in GPS radio occultation measurements, *J. Geophys. Res.*, *110*, D03102, doi:10.1029/2004JD005006.

Randel, W. J., and M. Park (2006), Deep convective influence on the Asian summer monsoon anticyclone, and associated tracer variability observed with Atmospheric Infrared Sounder (AIRS), *J. Geophys. Res.*, *111*, D12314, doi:10.1029/2005JD006490.

Reid, G. C. (1996), The tropical tropopause over the western Pacific: Wave driving, convection and the annual cycle, *J. Geophys. Res.*, *101*, 21,233–21,241.

Rocken, C., et al. (1997), Analysis and validation of GPS/MET data in the neutral atmosphere, *J. Geophys. Res.*, *102*, 29,849–29,866.

Santer, B. D., et al. (2003), Contributions of anthropogenic and natural forcing to recent tropopause height changes, *Science*, *301*, 479–483.

Sausen, R., and B. D. Santer (2003), Use of changes in tropopause height to detect human influences on climate, *Meteorol. Zeitschrift*, *12*, 131–136.

Schmidt, T., G. Beyerle, S. Heise, J. Wickert, and M. Rothacher (2006), A climatology of multiple tropopauses derived from GPS radio occultations with CHAMP and SAC-C, *Geophys. Res. Lett.*, *33*, L04808, doi:10.1029/2005GL024600.

Schneider, T. (2004), The tropopause and the thermal stratification in the extratropics of a dry atmosphere, *J. Atmos. Sci.*, *61*, 1317–1340.

Seidel, D. J., R. J. Ross, J. K. Angell, and G. C. Reid (2001), Climatological characteristics of the tropical tropopause as revealed by radiosondes, *J. Geophys. Res.*, *106*, 7857–7878.

Seidel, D. J., and W. J. Randel (2006), Variability and trends in the global tropopause estimated from radiosonde data, *J. Geophys. Res.*, *111*, D21101, doi:10.1029/2006JD007363.

Shapiro, M. A. (1978), Further evidence of the mesoscale and turbulent structure of upper level jet stream–frontal zone systems, *Mon. Weather Rev.*, *106*, 1100–1110.

Shapiro, M. A. (1980), Turbulent mixing within tropopause folds as a mechanism for the exchange of chemical constituents between the stratosphere and troposphere, *J. Atmos. Sci.*, *37*, 994–1004.

Shepherd, T. G. (2002), Issues in stratosphere-troposphere coupling, *J. Meteorol. Soc. Japan*, *80*, 769–792.

Sprenger, M., et al. (2003), Tropopause folds and cross-tropopause exchange: A global investigation based upon ECMWF analyses for the time period March 2000 to February 2001, *J. Geophys. Res.*, *108*(D12), 8516, doi:10.1029/2002JD002587.

Stohl, A., et al. (2003), Stratosphere-troposphere exchange: A review, and what have we learned from STACCATO?, *J. Geophys. Res.*, *108*(D12), 8516, doi:10.1029/2002JD002490.

Thuburn, J., and G. C. Craig (2002), On the temperature structure of the tropical substratosphere, *J. Geophys. Res.*, *107*(D2), 4017, doi:10.1029/2001JD000448.

Uppala, S. M., et al. (2005), The ERA40 reanalysis, *Quart. J. Roy. Met. Soc.*, *131*, 2961–3012.

Varotsos, C., C. Cartalis, A. Vlamakis, C. Tzanis, and I. Keramitsoglou (2004), The long-term coupling between column ozone and tropopause properties, *J. Climate*, *17*, 3843–3854.

Wernli, H., and M. Bourqui (2002), A Lagrangian "1-year climatology" of (deep) cross-tropopause exchange in the extratropical Northern Hemisphere, *J. Geophys. Res.*, *107*(D2), 4021, doi:10.1029/2001JD000812.

Wickert, J., et al. (2005), GPS radio occultation with CHAMP and GRACE: A first look at a new and promising satellite configuration for global atmospheric sounding, *Ann. Geophysicae*, *23*, 653–658.

Wirth, V. (2001), Cyclone-anticyclone asymmetry concerning the height of the thermal and the dynamical tropopause, *J. Atmos. Sci.*, *58*, 26–37.

World Meteorological Organization (1957), Meteorology — A three-dimensional science: Second session of the Commission for Aerology, *WMO Bulletin*, *vol. IV*(no. 4), 134–138.

WMO (2003), Scientific Assessment of Ozone Depletion: 2002. Global Ozone Research and Monitoring Project Report No. 47. World Meteorological Organization, Geneva, Switzerland.

L. L. Pan and W. J. Randel, National Center for Atmospheric Research, Boulder, CO 80307, USA. (randel@ucar.edu)

D. J. Seidel, NOAA Air Resources Laboratory, Silver Spring, MD 20910, USA.